AUTOMATIC ONBOARD DETECTION OF PLANETARY VOLCANISM FROM IMAGES. Brian Bue[1], Kiri Wagstaff[1], Rebecca Castano[1], Ashley Davies[1], [1]Jet Propulsion Laboratory, California Institute of Technology, 4800 Oak Grove Drive, Pasadena CA, 91109-8099, USA (Brian.D.Bue@jpl.nasa.gov, Kiri.Wagstaff@jpl.nasa.gov, Rebecca.Castano@jpl.nasa.gov, Ashley.Davies@jpl.nasa.gov)

Abstract: A computationally efficient algorithm for detecting volcanic plumes from image data has been developed and tested using several widely used image datasets. The algorithm is functional for images of both spherical and elliptical bodies and is currently able to correctly detect 78% of plumes in the test data. The accuracy and efficiency of the algorithm are assessed on a set of 60 Voyager 2, Galileo and Cassini images.

Introduction: In recent years, there have been numerous detections of volcanic or cryovolcanic activity on several bodies in the solar system [1,2,3]. These detections are of high scientific interest as they indicate dynamic endogenic processes occurring on those bodies.

However, there are problems with manually detecting these phenomena in imagery. First and foremost, inspecting individual images is a time-consuming and arduous process. Additionally, the inspection of these images could potentially take place long after events of interest occurred, which may result in lost opportunities for capturing significant science events. Consequently, we have investigated options for analyzing these images automatically onboard the spacecraft.

There are several principal benefits of doing onboard detection. Unsupervised data collection could be performed for extended time periods, which could also enable rapid response tasks (such has high frequency event monitoring when an event of interest occurs). Also, image prioritization could be performed in order to optimize downlink bandwidth usage.

Data: We focus on three separate datasets for testing our plume detection algorithm, two of which contain observations of the Jovian moon Io, and one that captures images of Saturn's moon Enceladus. The instruments that observed Io include the Voyager 2 Imaging Science Subsystem Narrow Angle Camera and Galileo's Solid State Imaging system. Cassini's Imaging Science Subsystem Narrow Angle Camera collected the Enceladus images.

Algorithm: The plume detection algorithm involves four principal steps. First, the image intensities are thresholded via a histogram analysis technique. Then the planetary limb and terminator points are extracted from the closed contour of the thresholded body. Next, an iterative ellipse fitting process is applied using the extracted limb points. Finally, radial profiles are calculated and thresholded to locate potential plumes within the image. Figures 1 through 4 illustrate this process. Here we describe the process in more detail.

1. Histogram Segmentation. Given a grayscale image of the planetary body of interest, we use the "triangle algorithm" developed by Zack et al [4] to estimate a per-image ideal threshold value. The image is then binarized using this threshold, which creates a set of connected components defined by the high-intensity pixels. These components are then subjected to morphological filtering to eliminate any artifacts from the thresholding.

2. Limb/Terminator Discrimination. Next, it is necessary to differentiate between "limb" (exterior) and "terminator" (interior) points on the body. This can be achieved using a technique developed by Udomkesmalee et al [5]. The closed contour of the planetary body is modeled using parametric functions as follows:

$$x(t) = R_x \sin(2\pi t + \phi) + \mu_x$$

$$y(t) = R_y \cos(2\pi t + \phi) + \mu_y$$

where R_x and R_y are ellipse radii, t is a parametric variable in the range [0,1], ϕ is the phase shift caused by selecting an arbitrary starting point on the contour, and (μ_x, μ_y) is the center of the ellipse. The intent is to "synchronize" the observed contour points with the parameterization, since the points that match well with the parameterization will lie on the exterior of a best-fit ellipse (yielding the limb points). This amounts to a matching process similar to a Hough transform [6] that involves a quadratic search in the elliptical case, and a linear search in the spherical case (since $R_x = R_y$).

3. Ellipse Fitting. The limb points are then used in a least-squares ellipse (or circle) fitting routine. First, an initial fit is calculated solely from the detected limb points. Since it is possible that some of the limb points went undetected in the limb/terminator discrimination step, a constrained radial scan using the initial fit is performed to better estimate the best fit ellipse/circle for the body.

4. Plume Detection via Radial Profiling. The creation of radial profiles occurs in unison with the radial scanning process. A radial profile is an ordered set of distances calculated from the center of the best-fit ellipse. In the circular case, a region is identified as a prospective plume if it is T positive standard deviations away from the mean of the profile distances, where T is a user-defined "detection threshold." In the elliptical

case, a similar process is performed using the best fit ellipse distances instead of the mean, and also taking angular positions into consideration when comparing profile distances.

Accuracy: In order to assess the accuracy of the algorithm, a suite of 60 images spanning each of the three datasets was collected. Each image was manually labeled to indicate the presence of a plume. These images were then processed by varying the detection threshold *T* in the range [0.0, 3.0]. Table 1 gives some selected results of the process. In the best case, 78.57% of the images with plumes are correctly identified, with a 22% false alarm rate.

It should be noted that the detection threshold can be tuned to the application at hand. For example, if the science requirements for a particular mission require that no plumes be missed (but false detections are less of a concern), then the threshold can be set accordingly. Alternatively, if the mission requires that no false detections occur (but missing some potential plumes is acceptable), then the threshold can be set using those criteria.

Threshold	*Percent Missed*	*False Detections*
1.55	9.07 %	12.36 %
2.10	0.076 %	53.57 %
> 2.90	75 %	0 %

Table 1: Selected thresholds and corresponding detection results.

Efficiency: Since this algorithm is intended for execution on a spacecraft, efficiency is a major concern. Current spacecraft processors are very limited in terms of processing capabilities in comparison to standard personal computers. The plume detection algorithm was designed with these criteria in mind, and table 2 gives the average runtimes for processing individual images from each of the selected datasets. The discrepancy in runtimes between the Voyager 2 and Galileo images is a result of additional morphological filtering that is necessary for processing the Galileo images.

	Image Dims	*Real*
Voyager 2	800x800	0.548s
Galileo	800x800	0.637s
Cassini	1024x1024	0.723s

Table 2: Average runtimes to process an image from each dataset on a MacBook Pro 2.16Ghz.

Conclusions: An algorithm for automated onboard plume detection from imagery was presented. The algorithm can be tailored to the needs of the application at hand via a user-definable detection threshold. Results from testing the algorithm using several datasets are yielding promising results.

Acknowledgements: The author would additionally like to thank Gabriel Udomkesmalee, Tim Stough, and William Owen for their assistance and suggestions on this project. This work was sponsored by the Interplanetary Network Directorate, and was performed at the Jet Propulsion Laboratory, under a contract with the National Aeronautics and Space Administration.

References:

[1] Porco, C., Helfenstein, P., Thomas, P., et al, "Cassini Observes the Active South Pole of Enceladus", *Science*, 311, 1393-1401, 2006.

[2] Geissler, P. and Goldstein D., "Plumes and Their Deposits", *Io After Galileo,* Ed. Lopes, R. and Spencer, J., Praxis Publishing, 2005.

[3] Strom, R. and Schneider, N., "Volcanic Eruption Plumes on Io", *Satellites of Jupiter,* Ed. Morrison, D., Univ. of Arizona Press, 1982.

[4] Udomkesmalee, S., Zhu, D. Q., and Chu, C., "Image Processing for Planetary Limb/Terminator Extraction", *Computer Vision and Image Understanding,* 67 (3), 274-284, 1997.

[5] Zack, G. W., Rogers, W. E. and Latt, S. A., "Automatic Measurement of Sister Chromatid Exchange Frequency", *Journal of Histochemistry and Cytochemistry* 25 (7), pp. 741-753, 1977.

[6] Duda, R. and Hart P. E., "Use of the Hough Transformation to Detect Lines and Curves in Pictures," *Comm. ACM*, 15, 11–15 (1972).

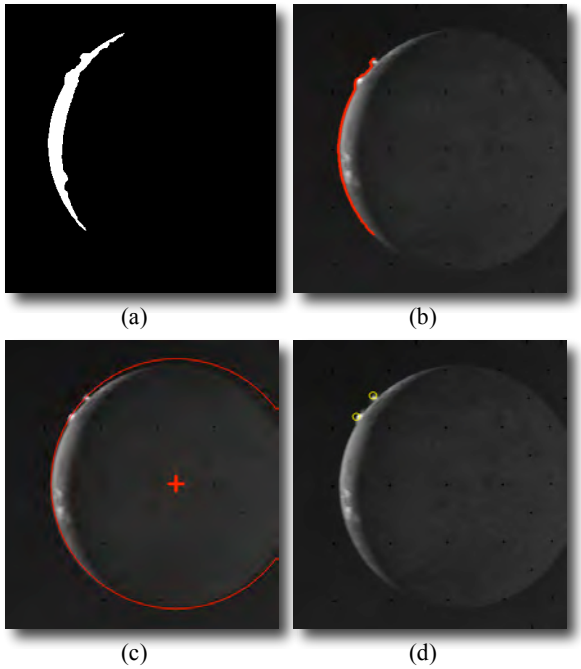

Figures a-d: Plume Detection Process. (a) image segemented via histogram analysis. (b) limb points are extracted from the closed contour of the segmented connected components. (c) circle/ellipse fitting is performed. (d) plumes detected by examining distances from the best fit circle/ellipse center